DOI：10. 13471/j. cnki. acta. snus. 2023B010

The high-temperature mechanical response of solid-state core monolith under operating condition*

LIANG Lichuang[1], *TIAN Jun*[2], *SU Dongchuan*[2], *LI Hui*[2], *JIANG Naibin*[1]✉

1. *Sino-French Institute of Nuclear Engineering and Technology, Sun Yat-sen University, Zhuhai 519082, China*
2. *Key Laboratory of Nuclear Reactor System Design Technology, Nuclear Power Institute of China, Chengdu 610213, China*

Abstract: The mechanical properties of heat pipe-cooled reactor which is a preferred core for nuclear reactor batteries at high temperatures needs attention. Taking MegaPower as the object, a thermal-mechanical coupling calculation of the reactor under full power operation condition is carried out using the open source Monte Carlo program (OpenMC) and ANSYS mechanical. The results show: (1) The core monolith generates significant temperature and thermal stress concentration, with peak temperatures of 1 023 K for the fuel and 970 K for the monolith, and the highest thermal stress of 49.5 MPa for the monolith; (2) Because of the effect of high-temperature creep, the stress in the monolith decreases significantly, and the stress distribution tends to be uniform. (3) During the core operation, the total equivalent strain of the monolith changes slightly, while the reduction of the equivalent elastic strain and the increase of the equivalent creep strain is almost simultaneous and equal.

Key words: solid-state reactor core; high temperature; 316H stainless steel; creep

CLC number: T341 **Document code:** A **Article ID:** 2097 − 0137(2024)02 − 0095 − 13

1 Introduction

Reactor power which has the advantages of high energy density, small size, high mobility and environmental adaptability, is the optimal solution to energy supply problems in the deep sea, deep space, and remote areas (Cai et al. , 2018). Among them, heat pipe-cooled reactors are considered one of the preferred reactor power supply types (Yan et al. , 2020). Los Alamos National Laboratory (LANL) and Westinghouse Electric Company have proposed megawatt-level heat pipe micro-reactors, MegaPower and eVinci respectively. These reactors can be transported by vehicle to provide highly reliable energy security for remote bases (Mc clure et al. , 2015; Arafat et al. , 2019). Concurrently, relevant domestic institutions have conducted extensive research on heat pipe reactor design for space, oceanic and terrestrial applications as well as heat pipe technology (Yu et al. , 2019; Qiu et al. , 2022). There are significant differences between heat pipe-cooled reactors and conventional reactors: (i) solid-state core; (ii) passive heat transfer of heat pipes; (iii) high

* **Received**: 2023 − 03 − 21 **Accepted**: 2023 − 04 − 07 **Published online**: 2023 − 07 − 03
Supported by Key Laboratory of Nuclear Reactor System Design Technology（HT-KFKT-24-2021015）

✉ **Corresponding author**: JIANG Naibin（*jiangnb@mail.sysu.edu.cn*）
LIANG Lichuang（*lianglch5@mail2.sysu.edu.cn*）；TIAN Jun（*tianjunhd@163.com*）；SU Dongchuan（*sdc03@139.com*）；
LI Hui（*757529786@qq.com*）

operating temperature; and (iv) fast neutron reactors with a hard neutron energy spectrum (Ma et al. , 2020). Therefore, conventional reactors' austenitic stainless steel 304L and 316L cannot meet the performance requirements of heat pipe reactors during high-temperature operation. The higher carbon content of 316H delivers higher tensile and yield strength than 316/316L. Due to its excellent high-temperature performance too, 316H stainless steel is widely used in fast reactors (Horak et al. ,1983).

Ma et al. (2021) proposed a new method that takes into account the geometric update and reactivity feedback of the solid core expansion. Based on the above mentioned, he constructed a neutron physics/thermal/mechanics three-field nuclear thermal coupling analysis program. Liu et al. (2022) conducted preliminary thermal and mechanical analyses on a new heat pipe-cooled reactor called NUSTER (nuclear silence thermoelectric reactor). Safety limits were proposed for NUSTER and the reactor's thermal and mechanical characteristics were analyzed under normal conditions and heat pipe failure accidents. In summary, recent research has focused on numerical analyzing of the thermal-hydraulic properties of heat pipe-cooled reactors under steady-state and startup conditions. These studies provide valuable insights into the safety limits of heat pipe-cooled reactors such as NUSTER (Du et al. , 2021; Tang et al. , 2022). For the solid-state core of the heat pipe-cooled reactor, the core monolith often needs to undertake the task of containing radioactive materials. Therefore, the reliability of the monolith plays an important role in the operation process of the reactor. Considering that the heat pipe-cooled reactor monolith cannot be replaced during its service period (5-15 years), it is necessary to analyze its stresses and deformations during its operation to ensure that the monolith does not fail. On the influence of high temperature and irradiation, the core monolith would undergo significant creep deformation. For the solid-state cores, creep could:

(1) Modify the core structure, and then influencing the distribution of neutron flux and power density. This may result in localized overheating or diminished power .

(2) Alter the contact between core components, and then impacting heat conduction and thermal impedance distribution. This may lead to an increase in temperature gradient or temperature peak .

(3) Induce relative displacement between core components to change, and then affecting the insertion and withdrawal of control rods and safety rods. This may result in decreased control precision or failure of safety guarantees.

However, there have been few reports on the creep behavior of heat pipe-cooled reactor cores. In this study, ANSYS mechanical software was used to perform thermal-mechanical coupling calculations on a typical solid-state heat pipe-cooled reactor, MegaPower. The aim is to simulate its high-temperature mechanical behavior under full-power steady-state operation conditions and compare the stress and strain changes in the core monolith while taking creep effects into consideration.

2 Physical model and method

The core structure of MegaPower with a thermal power of 5 MW is shown in Fig. 1 (Mcclure et al. , 2015). The MegaPower core is hexagonal in shape and consists of six identical trapezoidal columns with air gaps between them to accommodate thermal expansion. The trapezoidal columns have a large number of deep holes in regular rows to accommodate the heat pipes and fuel rods. The base of the trapezoidal column is made of stainless steel 316H, the fuel rods are made of UO_2, and the gaps between fuel rods and the trapezoidal column are filled with He.

According to reactor geometry parameters in the reference (Romano et al. , 2013), neutron transportation is calculated by OpenMC. The axial power distribution of each fuel rod in the core is obtained in this simulation process. Then, thermal-mechanical coupling calculations of the core is conducted using ANSYS mechanical based on the power density distri-

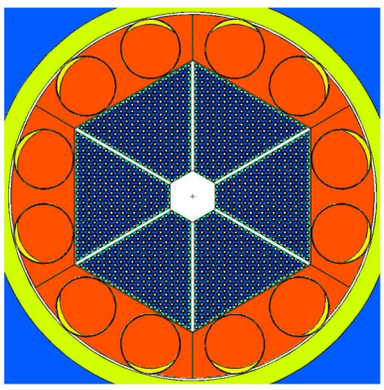

Fig. 1 Schematic diagram of the arrangement of the core

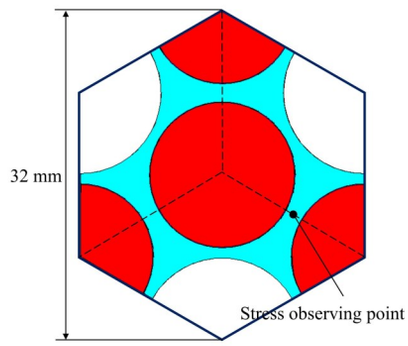

Fig. 3 Grid-independent verification element

bution (as shown in Fig.2). The repeating element inside MegaPower (as shown in Fig. 3) is chosen for grid-independent analysis, and the Von Mises stress at the stress observing point is used to compare the effects of grid refinement on the computational results.

To balance the computational accuracy and cost, the 1/6 core of MegaPower is taken for 3D modeling. Comparing the variation of Von Mises stress with the element size, the computational results difference is not apparent when the plane element size is refined to 0.1 mm. Therefore, the element size within the cross-section is set to 0.1 mm. Solid thermal-structural coupled element SOLID90 is used, and the finite element model there's a total of 2.7 million elements and 7 million nodes is shown in Fig.4.

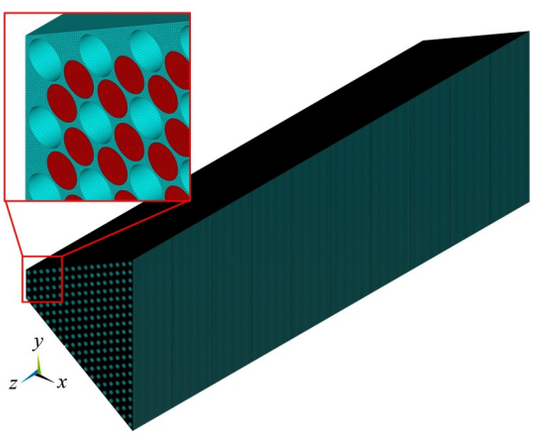

Fig. 4 Finite element model of the reactor core

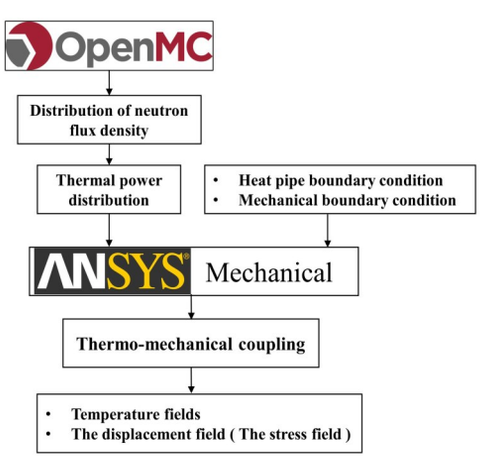

Fig. 2 Schematic diagram of calculation process

monolith are set as adiabatic boundary conditions; the power density distribution obtained from OpenMC neutron transport calculations is loaded onto each corresponding fuel rod as heat sources, as show as Fig.5.

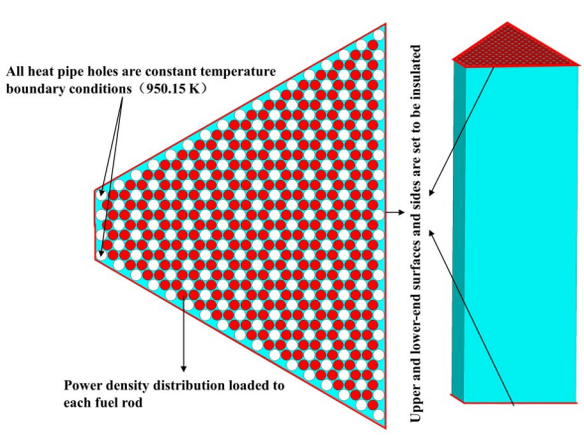

Fig. 5 Boundary conditions of finite element models

3 Simulation results

3. 1 MegaPower reactor monolith thermal analysis

All sides, upper and lower end surfaces of the

Axial middle profile and symmetric profile of the 1/6 core are selected to observe the temperature distribution of the solid-state core, as shown in Fig.6. The temperature distribution of the core is shown in

Fig. 7. The peak temperature of the fuels is 1 023 K, which is about 73 K higher than the core heat trap (950.15 K). The overall temperature distribution of the core shows a high center and low outside in both directions, and the presence of the radial reflection layer increases the power distribution density outside of the core, and then resulted in a considerable temperature increase in these regions.

Fig. 8 shows the temperature distribution of the core monolith. The temperature near the center and the reflector layer is relatively high. The webs between the fuel form a high-temperature concentration due to the accumulation of significant sensible heat. To examine the axial temperature of the high-temperature concentration webs, the center of the web is selected as the axial path (path-1), see Fig. 9. The temperature distribution on path-1 shows a cosine distribution. The neutron reflection performance in upper reflection layer of the core with a large number of holes is lower than that of the bottom reflection layer without holes. Therefore, the temperature at the bottom of the core is higher than that at the top.

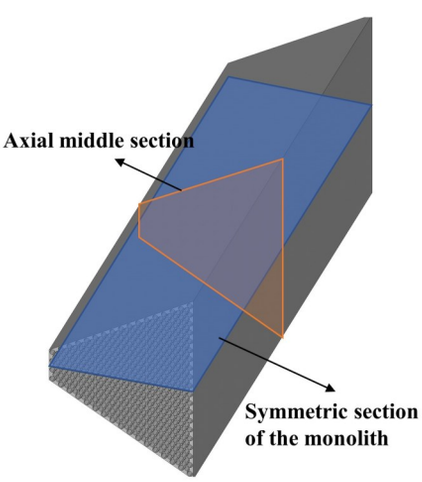

Fig. 6 The selection profiles of the finite element model

3. 2 Mechanical analysis of solid-state core monolith

Considering the placement of the core monolith in the reactor, a single-point fixed constraint is applied to inner center on the bottom surface; weak spring constraints are applied to both UX and UZ directions of the inner side and bottom surface, as shown in Fig.10.

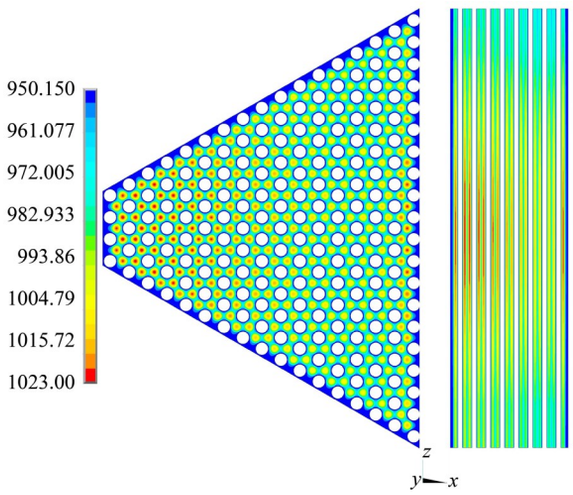

Fig. 7 Temperature distribution of the core (unit: K)

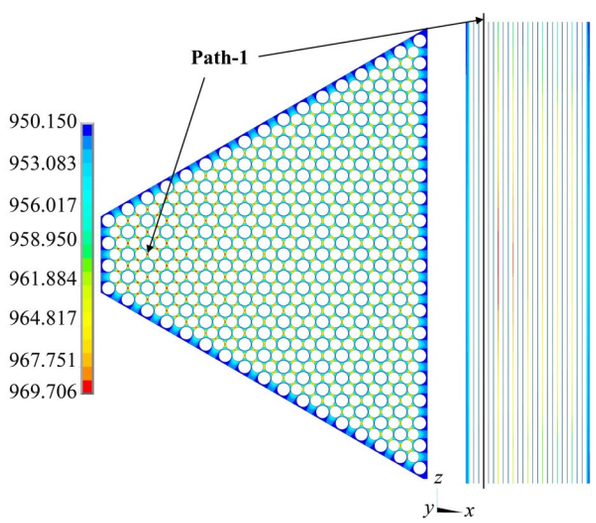

Fig. 8 Temperature distribution of the core monolith (unit: K)

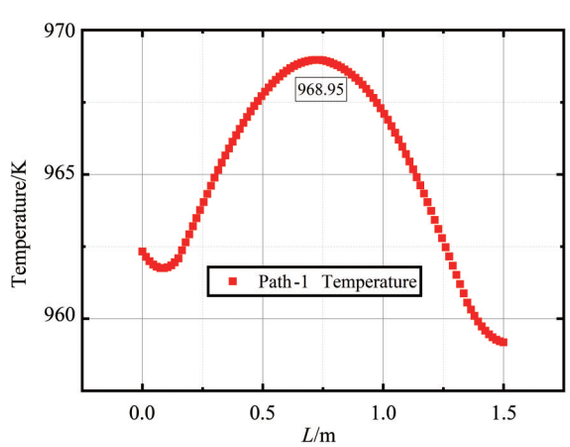

Fig. 9 Temperature change curve of path-1

The distribution of Von Mises stress in the axial middle section of the monolith is shown in Fig. 11. There is a "thermal stress concentration" in the webs

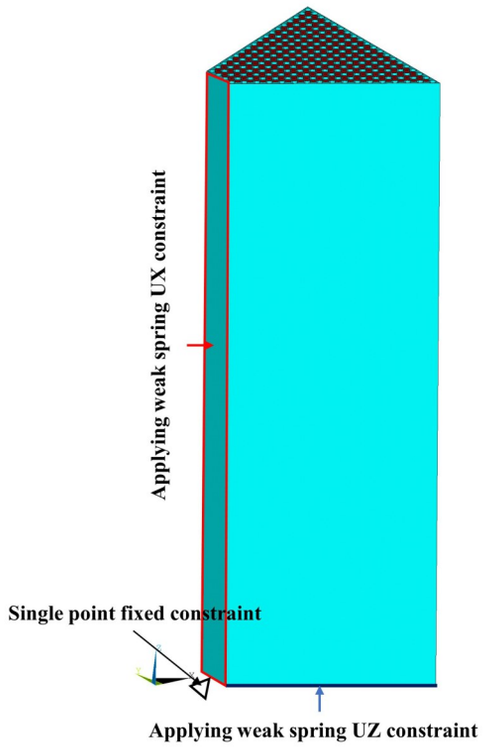

Fig. 10 Boundary conditions of finite element models

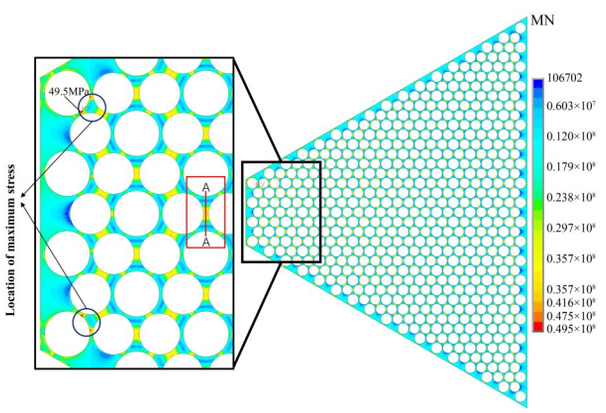

Fig. 11 Stress distribution in the axial middle section of the core monolith

between adjacent fuels, which overlaps with the "high-temperature concentration" areas.

The stress distribution of path-1 is shown in Fig. 12. From Fig. 12(a), it's obvious that the thermal stress component of SZ direction (axial stress) is domaint, while the stress components of SX and SY direction are smaller. All the stress components on the path are compressive except for SY near the two end faces, which are tensile. It is showed that the thermal stress distribution of SZ direction is more consistent with the Von Mises stress in Fig.12(b).

To analyze the "stress concentration" phenomenon of a fuel-to-fuel web, one of the webs with stress concentration is chosen in Fig. 11. The relationship between the temperature distribution and the stress distribution in chosen A – A section is shown in Fig. 13. In the picture, because of the influence of temperature inhomogeneity, the adjacent low-temperature region suppresses the thermal expansion in the axial direction in the high-temperature concentration region, thus accumulating a large axial compressive stress.

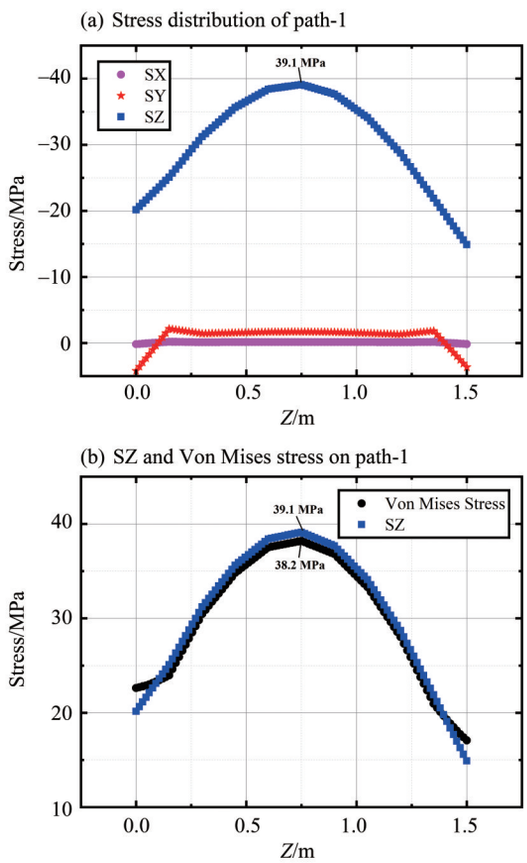

Fig. 12 Stress distribution curve of path-1

It is shown in Fig.14 that how temperature distribution affects stress distribution in the middle profile of the web. The high-temperature areas between adjacent fuels accumulate more sensible heat and suppress thermal expansion toward the heat pipe hole by the heat trap (heat pipe) boundary. This leads to considerable stress concentration in the web between the heat pipe and fuel.

In Fig. 11, the maximum Von Mises stress of

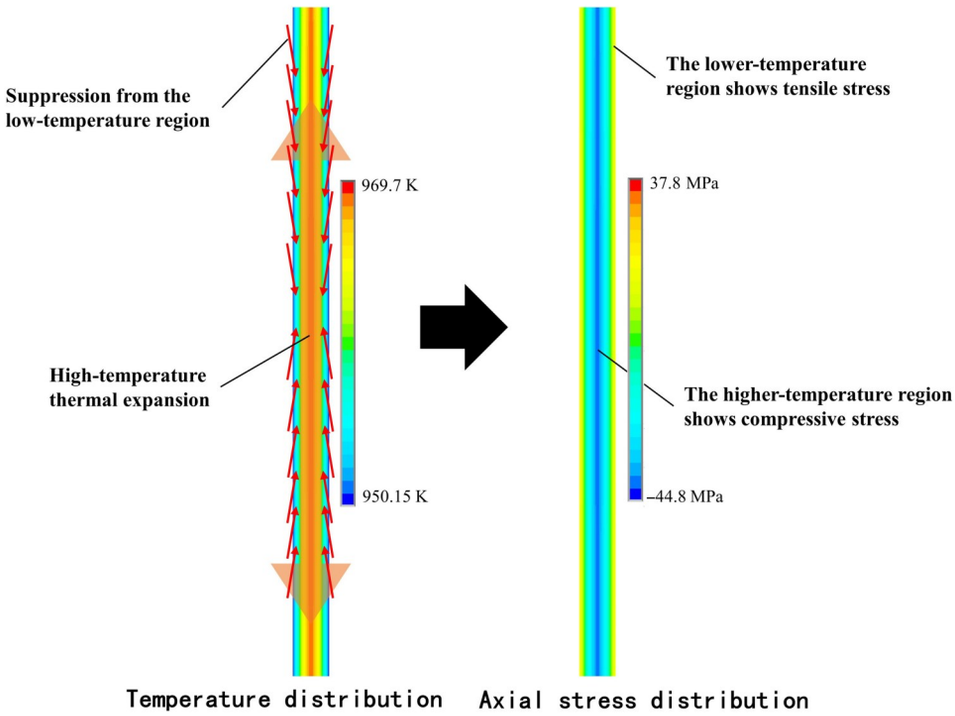

Fig. 13 Axial stress in A–A section

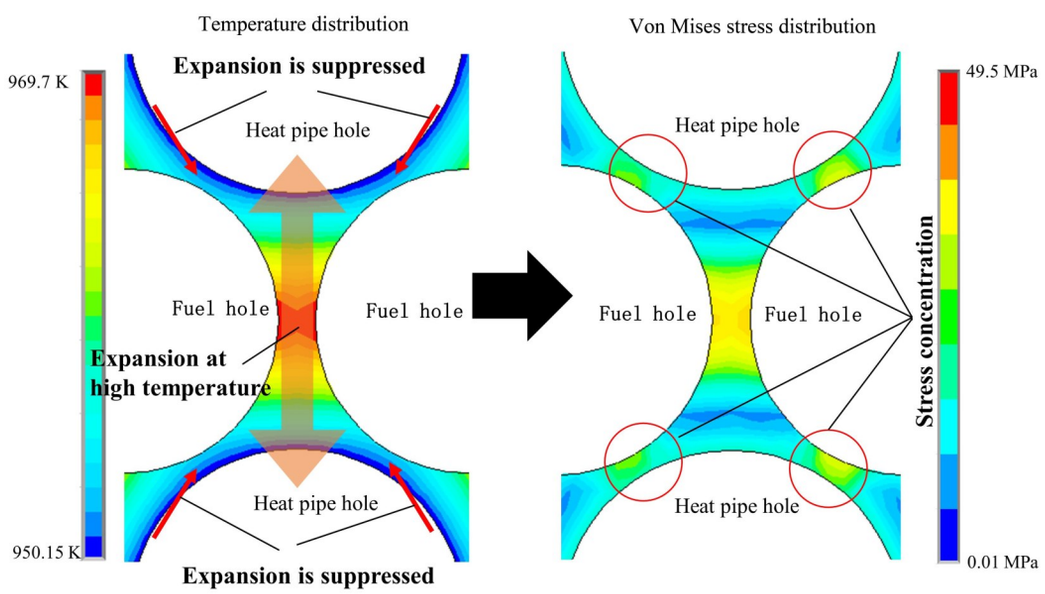

Fig. 14 Stress of stress-concentrated monolith web

49. 5 MPa in the monolith occurs at the inner vertex of the heat pipe and adjacent fuel web, the temperature distribution of this region as shown in Fig. 15. The temperature of most region near the heat pipe hole is close to 950. 15 K, which is lower than the average temperature of the monolith and limits overall thermal expansion. In Fig. 15, the center of the heat pipe hole has significant circumferential stress concentration. Circumferential tensile stress is the main source of thermal stress at the web between the heat pipe and the adjacent fuel. It must be noted that the potential failure in this region may occurs due to the significant stress concentration.

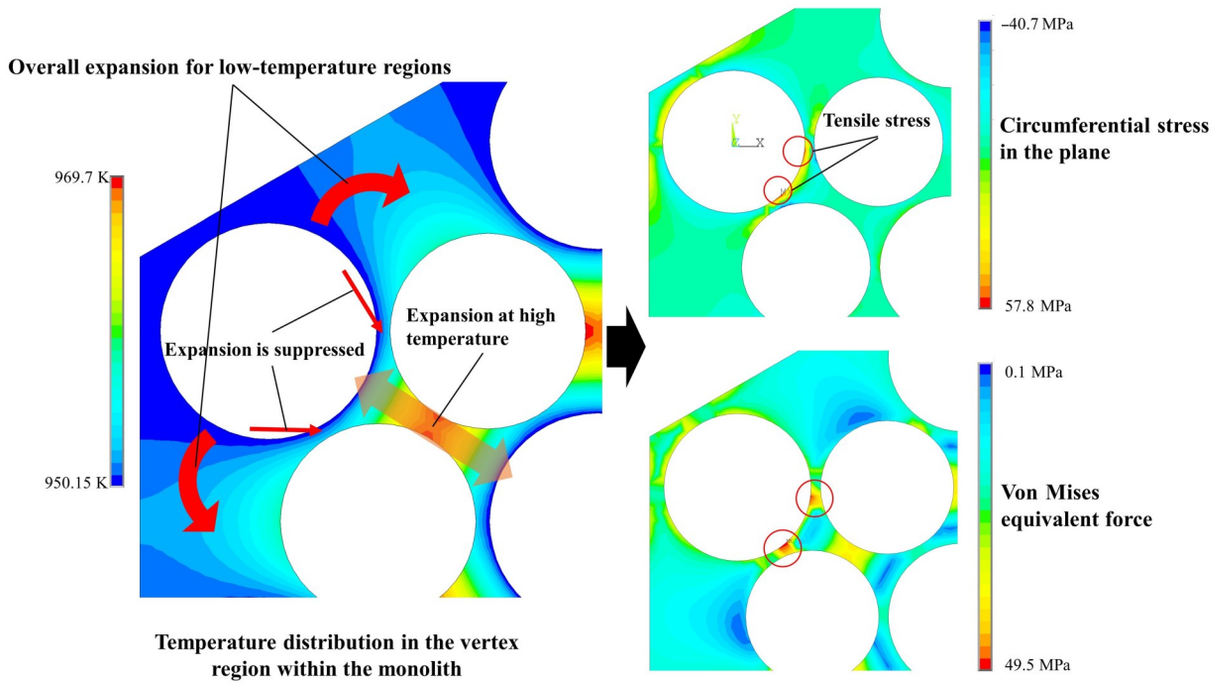

Fig. 15 Stress of the heat pipe hole near the vertex of the monolith

4 Creep mechanism

Creep occurs when solid materials undergo slow and irreversible plastic deformation under continuous stress (Betten et al. , 2008). Thermal creep could happen at temperatures up to 970 K for stainless steel. For the reactor core, the operating temperature of the monolith can reach 950~970 K. At such elevated temperatures, it is essential to consider the creep characteristics of the core monolith. A coupled creep model is used to calculate the stress and strain of the solid core under full power conditions, then the variation trend of the core during operation and effect of creep is studied in this paper.

4. 1 Creep constitutive model

The creep strain of material versus time t can be expressed by a creep curve. The creep effect can be divided into three stages: I-primary creep, II-secondary creep, and III - tertiary creep. Temperature and stress affect the duration of each stage and the size of the strain. The duration of the first stage becomes shorter when the temperature is higher, and the duration of the second stage is longer when the stress is lower. Within a certain range of temperature and stress, creep strain can be expressed as (Naumenko et al. , 2007):

$$\varepsilon_{cr} = f_1(t) f_2(T) f_3(\sigma), \tag{1}$$

where, ε_{cr} is the creep strain; $f_1(t), f_2(T), f_3(\sigma)$ is respectively the functions of time, temperature and stress.

During full power operation, the temperature of the core monolith of the MegaPower heat pipe reactor is 950~970 K, and the maximum stress is about 50 MPa. Under these conditions, the high-temperature creep of 316H stainless steel is mainly in the steady-state creep stage (Sikka et al. , 1980; Zhu et al. , 1983; Horak et al. , 1983; Whittaker et al. , 2012; Esposito et al. , 2016). In the steady-state creep stage, the creep rate $\dot{\varepsilon}_{cr}$ is often selected as the design index (Naumenko et al. , 2007). The relationship between $\dot{\varepsilon}_{cr}$ and σ is:

$$\dot{\varepsilon}_{cr} = C_1 \exp(\sigma / C_2), \tag{2}$$

where, C_1 and C_2 are material parameters, which are determined by the steady-state creep strain rate test at different temperatures. The 316H high-temperature creep data comes from the National Institute of Materials Science (NIMS, 1988). The creep model parameters are shown in Table 1.

Table 1 Material parameters of 316H stainless steel

Temperature/℃	Parameters	
	C_1	C_2
600	6.85×10^{-9}	18 671 690
650	2.68×10^{-8}	13 931 370
700	4.55×10^{-8}	9 820 220
750	8.05×10^{-8}	7 085 390
800	5.11×10^{-7}	5 760 131

From Fig. 11, it can be seen that the webs between the fuel in the red box show a significant thermal stress concentration phenomenon, and this part will be a key research object in the strength analysis of the core monolith. In order to reduce the computational cost, the repeating element of the middle section is selected to predict the high-temperature creep behavior of the monolith, as shown in Fig.16. The result of the linear-elastic thermal-mechanical coupling calculation is shown in Fig.17. Significant stress concentration is observed near sides of the heat pipe to the fuel (point-1 /point-2) web and the center of the fuel-to-fuel web (point-3). Von Mises stress distribution along the path for the repeating element and one-sixth models is contrasted in Fig.18. As can be seen, there is a slight deviation in the Von Mises stress. But the consistent distribution pattern indicated that the simplified element for predicting the high-temperature creep behaviors is reasonable.

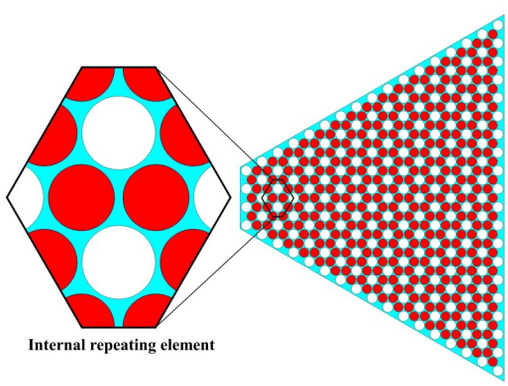

Fig. 16 Selection of repeating element

4. 2 Stress analysis

The stress distribution at 0, 100, 500 and 900 h in high-temperature creep process is shown in

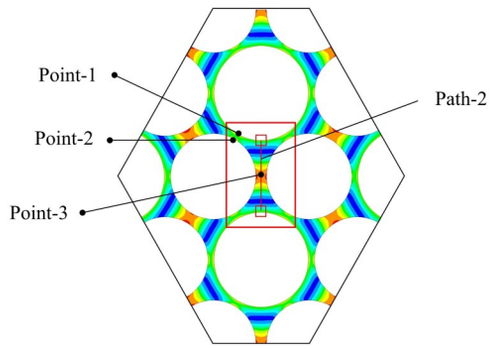

Fig. 17 Von Mises stress distribution of the repeating element, observation points and path

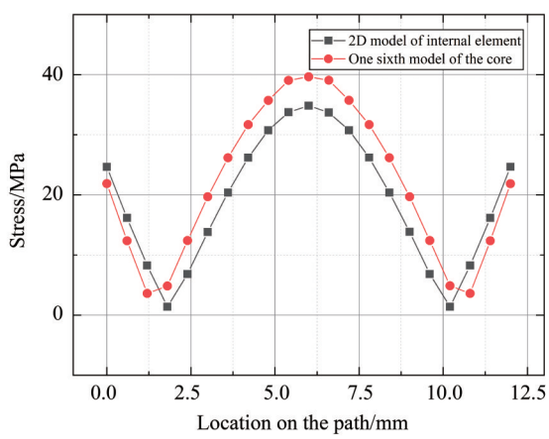

Fig. 18 Von Mises stress distribution along the path for the repeating element and one-sixth models

Fig. 19. The results showed that the distribution of Von Mises stress and SZ (axial stress component) become more uniform as time increase, and the stress concentration phenomenon is moderated. Fig. 21 illustrates the change of Von Mises stress at different parts over time. In the focus area (black box in Fig. 19 and Fig. 20), the Von Mises stress in the center of the fuel-to-fuel web decreased faster at the beginning, and then the stress decreased gradually. The Von Mises stress near the fuel side and the heat pipe side of the heat pipe to fuel web also decreased, but the decrease rate was more stable. Due to the variability of stresses and temperatures at each site, the location of the maximum Von Mises stress shifted from the center of the fuel-to-fuel web to the heat pipe side of the web between the heat pipe and the fuel.

Fig. 22 and Fig. 23 present the Von Mises stress and SZ distribution along the path under full power operation. We found that the SZ is the main stress

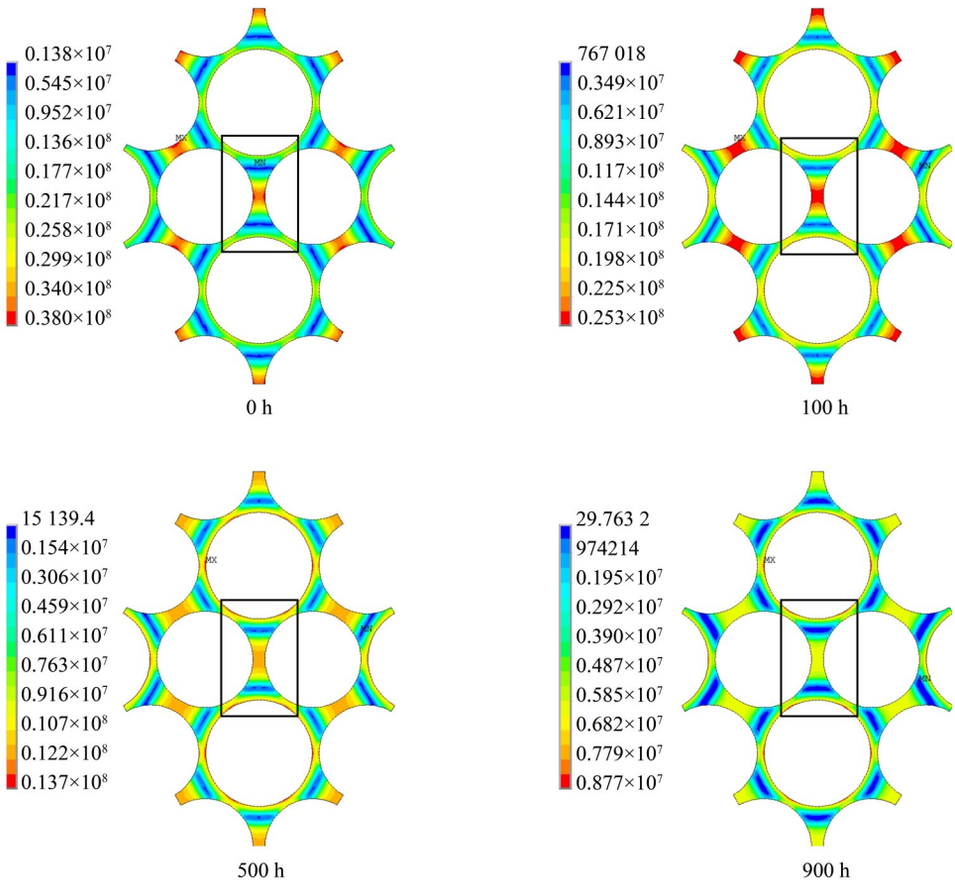

Fig. 19 Von Mises stress distribution at different moments

component of the Von Mises stress in the path. With the operation of the reactor, the stress became more uniform, and the stress in the middle of the path was already uniform at 900 h. However, the two sides of the path (heat pipe boundary) became parts with higher stress at the end of service life because the stress (mainly axial tensile stress) decreased slightly slower than that in the middle.

4. 3 Strain analysis

Fig.24 illustrate the equivalent strain and equivalent creep strain of the monolith at different moments. It is found that the equivalent strain barely changed under the effect of high-temperature creep, whereas the equivalent creep strain increased gradually. The creep strain increased most significantly at the center of the fuel-to-fuel web.

Fig. 25 displays the curves of equivalent effect strain, equivalent elastic strain and equivalent creep strain at point-1, point-2 and point-3. In the figure, it is noticed that the variation of the equivalent strain at these three locations was very small, and the equivalent strain at point-1 had a slight tendency to decrease during the reactor operation. Due to the effect of high-temperature creep, a part of the elastic strain was converted to creep strain when the total strain was considered to be almost constant, resulting in a decrease in the elastic force due to elastic strain, which in turn led to a decrease in the Von Mises stress. Moreover, the decrease in elastic strain and the increase in creep strain occurs at the same time of equal number.

Fig.26 and Fig.27 illustrate the equivalent creep strain and equivalent elastic strain distributions along the path at different moments. According to Fig.26, the creep strain in the middle of the path increased faster, and the creep strain distribution along the path become more and more uneven. As shown in Fig.27, as the creep strain continues to increase, the elastic strain tends to become relatively flat. At 900 hours, the elastic strain in the middle of the path

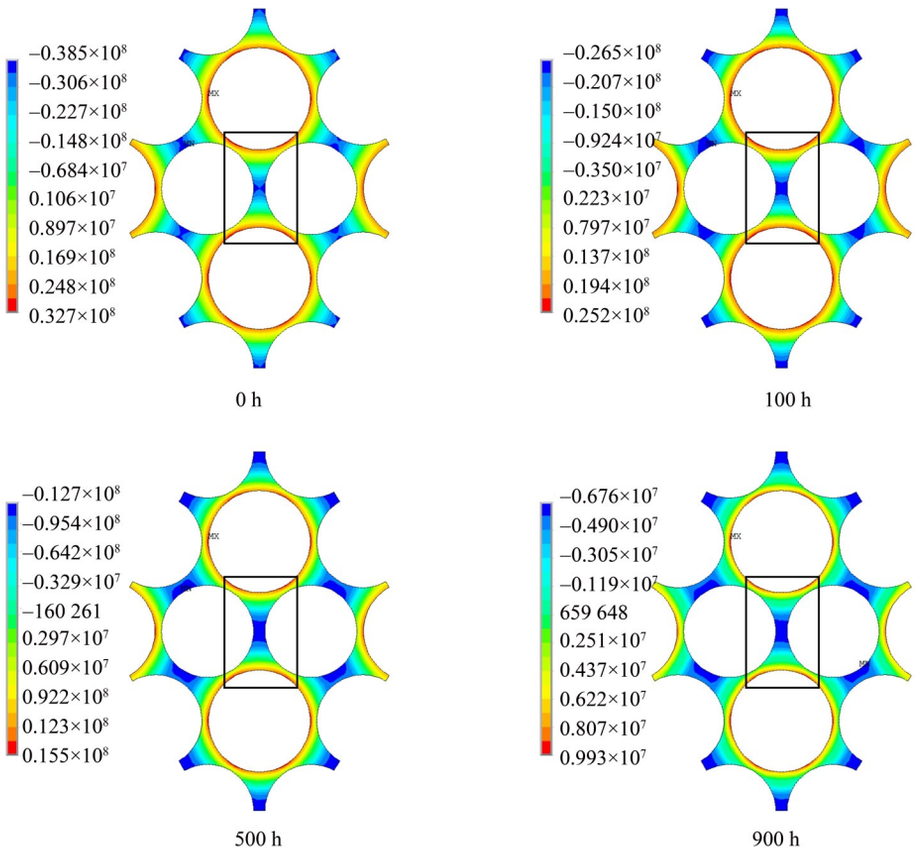

Fig. 20 SZ stress distribution at different moments

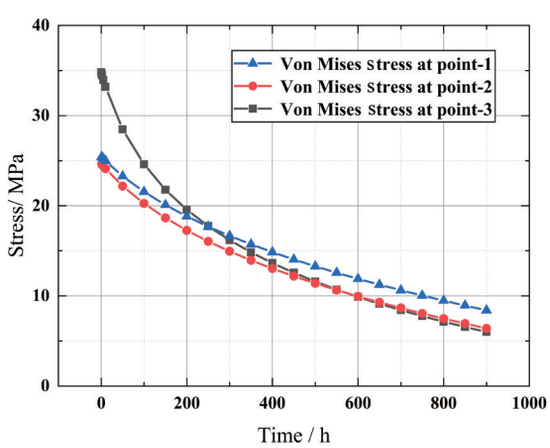

Fig. 21 Von Mises stress curve in different parts

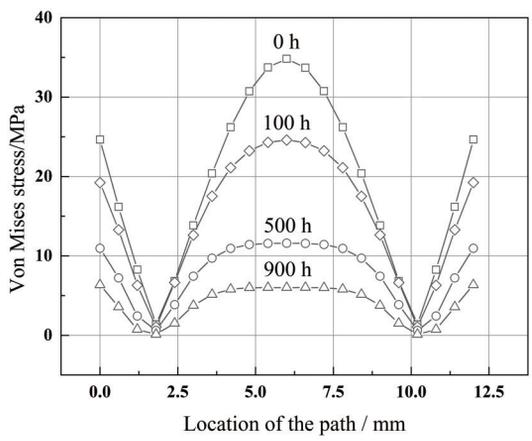

Fig. 22 Von Mises stress distribution along the path

has become consistent. It can be inferred that the elastic force caused by the elastic strain would also be flat.

5 Conclusion

In this study, the high-temperature mechanical behavior of the solid-state core monolith under full-power operation conditions is simulated by OpenMC and ANSYS mechanical.

Based on the linear-elastic thermal-mechanical coupling analysis of the 1/6 core model, the following conclusions are drawn:

(1) The core monolith exhibits substantial thermal concentration, resulting in highest temperatures of 970 K.

(2) The webbing between fuel and fuel is the

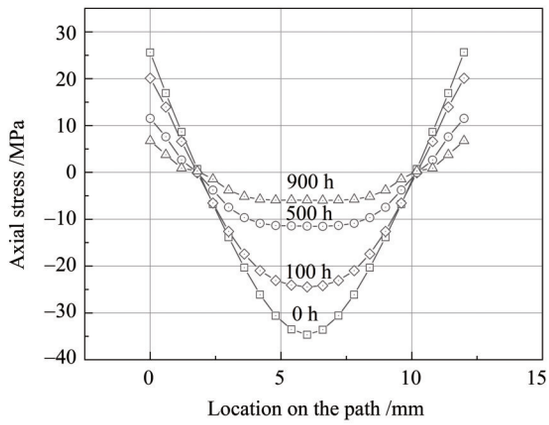

Fig. 23 Stress components distribution along the path SZ

high temperature and stress concentration areas, and the thermal stress components in these areas are mainly axial compressive stresses.

(3) The highest stress in the monolith is 49.5 MPa, which occurs at the webbing between the heat pipe and the adjacent fuel at the inner vertex of the monolith, and the main component of the stress is circumferential tensile stress.

Based on coupling the steady-state creep model, the following conclusions are drawn:

(1) With the operation of the reactor, the stress of the 316H stainless steel monolith of the core decreased, and the rate of stress decrease gradually slowed down.

(2) The monolith stress distribution tended to average out, and the site of maximum stress changed from the center of the web between the fuel and the fuel to the web between the heat pipe and the fuel.

(3) The distribution of the equivalent strain of the 316H stainless steel monolith hardly changed during operation, and the decrease in elastic strain and the increase in creep strain are almost simultaneous and equivalent under the effect of high-temperature thermal creep.

(4) The simplified calculation model in this pa-

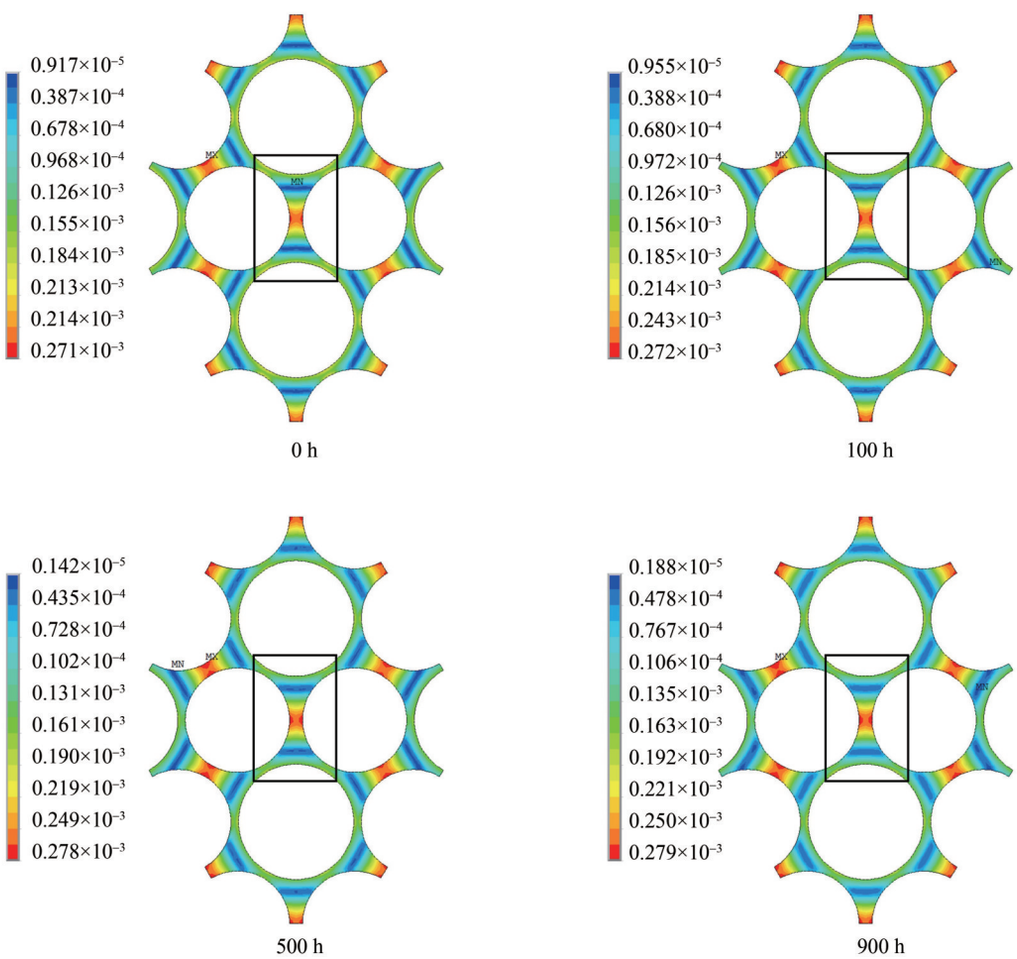

Fig. 24 Equivalent effect variation distribution

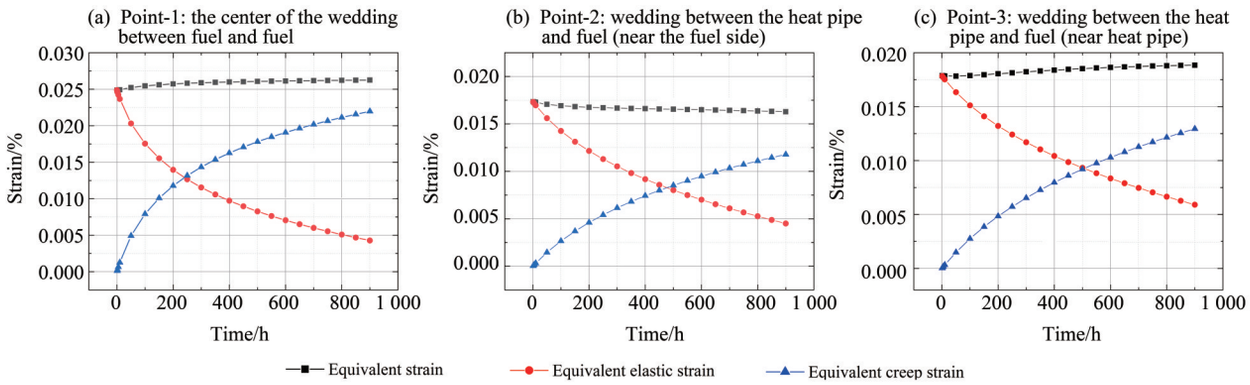

Fig. 25 Equivalent effective strain, equivalent elastic strain and equivalent creep strain in different parts

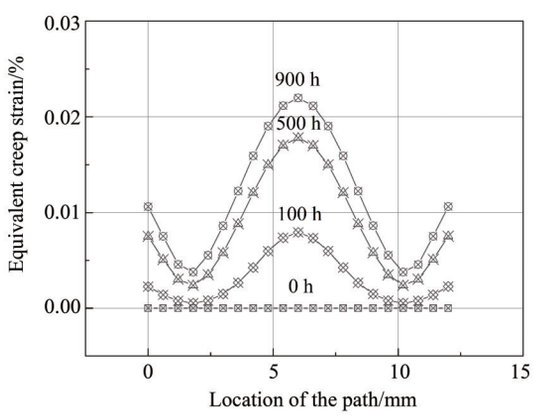

Fig. 26 Equivalent creep strain distribution along the path

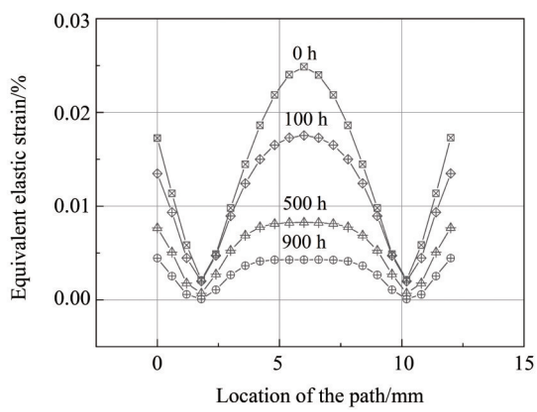

Fig. 27 Equivalent elastic strain distribution along the path

per is reasonable in predicting the high-temperature creep behavior of the monolith. Considering the core irradiation effect, more accurate full-core calculations and mechanical behavior study needed further be carried out.

References:

ARAFAT Y, van WYK J, 2019. eVinci micro reactor[J]. Nuclear Plant Journal, 37(3):34-37.

BETTEN J, 2008. Creep mechanics[M]. Berlin:Springer.

CAI F, JI J M, JIANG Z Q, et al, 2018. Engineering fronts in 2018[J]. Engineering, 4(6): 748-753.

DU X, TAO Y, ZHENG Y, et al, 2021. Reactor core design of UPR-s: A nuclear reactor for silence thermoelectric system NUSTER[J]. Nucl Eng Des, 383(6): 111404.

ESPOSITO L, BONORA N, de VITA G, 2016. Creep modelling of 316H stainless steel over a wide range of stress [J]. Procedia Struct Integr, 2:927-933.

HORAK J A, SIKKA V K, RASKE D T, 1983. Mechanical properties and microstructures of types 304 and 316 stainless steel after long-term aging[R]. Clinton: Oak Ridge National Lab.

LIU L, LIU B, XIAO Y, et al, 2022. Preliminary thermal and mechanical analysis on the reactor core of a new heat pipe cooled reactor applied in the underwater environment [J]. Prog Nucl Energy, 150:104306.

MA Y, LIU M, XIE B, et al, 2021. Neutronic and thermal-mechanical coupling analyses in a solid-state reactor using Monte Carlo and finite element methods[J]. Ann Nucl Energy, 151: 107923.

MA Y, LIU M, YU H, et al, 2020. Neutronic/Thermal-Mechanical coupling in heat pipe cooled reactor [J]. Nucl Power Eng, 41(4): 191-196.

MC CLURE P R, POSTON D I, DASARI V R, et al, 2015. Design of megawatt power level heat pipe reactors[R]. Los Alamos, United States: Los Alamos National Lab (LANL): 29.

NAUMENKO K, ALTENBACH H, 2007. Modeling of creep for structural analysis[M]. Berlin, Heidelberg: Springer

Science & Business Media.

NIMS，1988. NRIMS creep data sheet No. 42［R］. Japan：National Institute for Materials Science：1.

QIU S Z，ZHANG Z Q，ZHANG Z P，et al，2022. Study on thermal-hydraulic characteristics of ocean silent heat pipe cooled reactor［J］. At Energy Sci Technol，56（6）：989-1004.

ROMANO P K，FORGET B，2013. The OpenMC Monte Carlo particle transport code［J］. Ann Nucl Energy，51：274-281.

SIKKA V K，BOOKER B L P，BOOKER M K，et al，1980. Tensile and creep data on type 316 stainless steel［R］. Clinton：Oak Ridge National Laboratory.

TANG S，LIU X，WANG C，et al，2022. Thermal-electrical coupling characteristic analysis of the heat pipe cooled reactor with static thermoelectric conversion［J］. Ann Nucl Energy，168：108870.

WHITTAKER M T，EVANS M，WILSHIRE B，2012. Long-term creep data prediction for type 316H stainless steel［J］. Mater Sci Eng A，552：145-150.

YAN B H，WANG C，LI L G，2020. The technology of micro heat pipe cooled reactor：A review［J］. Ann Nucl Energy，135：106948.

YU H，MA Y，ZHANG Z，et al，2019. Initiation and development of heat pipe cooled reactor［J］. Nucl Power Eng，40（4）：1-8.

ZHU J H，BOERMAN D，PIATTI G，1983. Strength of the AISI 316 stainless steel above 800℃［C］// Transactions of the 7th International Conference on Structural Mechanics in Reactor Technology. Chicago，IIIinois，USA Elsevier Science Publishing Company：507-514.

运行工况下固态堆芯基体的高温力学响应

梁立创[1]，田俊[2]，苏东川[2]，李辉[2]，姜乃斌[1]

1. 中山大学中法核工程与技术学院，广东 珠海 519082
2. 中国核动力研究设计院核反应堆系统设计技术重点实验室，四川 成都 610213

摘要：热管冷却反应堆是核反应堆电池的首选堆芯之一，热管堆固态堆芯高温膨胀的力学性能需要引起重视。为了获得热管冷却反应堆316H不锈钢基体在高温下的力学变化，以MegaPower作为分析对象，采用开源蒙特卡罗程序（OpenMC）和商用有限元计算软件ANSYS Mechanical，对反应堆满功率运行工况进行了热力耦合分析。结果表明：1）在满功率运行水平，堆芯基体会产生显著的温度集中和热应力集中，燃料和基体的峰值温度分别为1 023 K和970 K，基体的最大热应力为49.5 MPa；2）在高温蠕变的效应下，基体的应力会显著降低，应力分布趋于均匀；3）在堆芯运行过程中，基体等效总应变只有微小变化，而等效弹性应变的减少和等效蠕变应变的增加几乎是同步且等量进行的。

关键词：固态堆芯；高温；316H不锈钢；蠕变

（责任编辑　王海蓉）